Article:
Guo, K.-L., Zhang, Y., Gu, J.-L. et al. (2026) Ultralarge elastic strain and near-constant stress temperature dependence of Ni–Mn–Ti–Fe–Co eutectic high-entropy alloy. Transactions of Nonferrous Metals Society of China, 36 (5). pp. 1597-1609. ISSN: 1003-6326

https://doi.org/10.1016/s1003-6326(26)67049-5

Contents lists available at ScienceDirect

Transactions of Nonferrous Metals Society of China

36(2026) 1597−1609

www.tnmsc.cn

Ultralarge elastic strain and near-constant stress temperature dependence of Ni−Mn−Ti−Fe−Co eutectic high-entropy alloy

Ke-liang GUO [a], Yu ZHANG [a], Jiang-long GU [b], Jing BAI [a,c,*], Dan LIU [a,c], Nicola MORLEY [d], Qing-shuang MA [c], Qiu-zhi GAO [c], Liang ZUO [a]

[a] Key Laboratory for Anisotropy and Texture of Materials (Ministry of Education), School of Materials Science and Engineering, Northeastern University, Shenyang 110819, China;

[b] State Key Laboratory of Metastable Materials Science and Technology, Yanshan University, Qinhuangdao 066004, China;

[c] Key Laboratory of Dielectric and Electrolyte Functional Materials of Hebei Province, School of Resources and Materials, Northeastern University at Qinhuangdao, Qinhuangdao 066004, China;

[d] Department of Material Science and Engineering, University of Sheffield, Sheffield, S1 3JD, UK

Abstract: The notable stress hysteresis and strong temperature dependence limit the application of superelastic alloys. In this study, we developed a Ni−Mn−Ti−Fe−Co superelastic high-entropy alloy system with low temperature dependence by integrating high-entropy alloy principles into the Ni−Mn−Ti system through arc-melting technology. By designing a fully eutectic microstructure, the alloy demonstrated stable superelasticity with minimal hysteresis energy dissipation, maintaining a 5% strain across a broad temperature range from 113 to 433 K. Furthermore, it exhibited fully reversible superelasticity of 5% after 12010 cycles at room temperature and demonstrated significant pseudoelasticity of about 8.2% under a high stress of 1600 MPa. Its excellent elasticity, minimal hysteresis energy dissipation, and near-constant stress−temperature dependence over a wide temperature range are attributed to its unique eutectic microstructure and weak first-order phase transformation, making it a promising candidate for applications requiring reliable superelastic performance across diverse temperature environments.

Keywords: high-entropy alloy; linear superelasticity; martensitic transformation; eutectic microstructure

1 Introduction

A wide variety of high-performance engineering applications, ranging from deep-space and deep-sea exploration to advanced robotics, require metallic components with remarkable ability to undergo substantial and reversible deformation over a broad temperature range [1,2]. The elastic limit of metallic materials is constrained by the crystal structure and metallic bond, resulting in the elastic limit of alloys rarely exceeding 1% [3,4], which greatly limits the applications of metallic materials in mechanical energy storage, precision control, and elastic strain engineering [5−7]. Metallic bonds exhibit a certain degree of elastic strain, which makes the metallic materials undergo reversible elastic deformation within a certain range of stress. However, metallic bonds have an elastic limit, beyond which the bonds may break or rearrange, resulting in permanent deformation. In contrast, alloys that exhibit stress-induced martensitic transformation (SIMT), such as NiTi-, Fe- and Cu-based shape memory alloys (SMAs) [8−10], can achieve significant recoverable

Corresponding author: *Jing BAI, Tel: +86-18233511369, E-mail: baijing@neuq.edu.cn

https://doi.org/10.1016/S1003-6326(26)67049-5

Received 3 September 2024; accepted 4 July 2025

pseudo-elastic strain of up to 10%, commonly referred to as superelasticity. However, the nature of SIMT makes the superelasticity have significant hysteresis and temperature dependence [11].

The hysteresis is not only detrimental to the recoverability of stored energy and precise control but also ultimately leads to material fatigue and failure [12−14]. The main reason for stress hysteresis during the loading and unloading process of SMAs is energy dissipation caused by martensitic/austenitic phase nucleation and interface expansion [15,16]. Constructing a heterogeneous structure within the alloy is pivotal to achieving quasi-linear large elastic strains. The slim stress hysteresis observed in quasi-linear superelastic alloys may be attributed to a significant reduction in martensitic nucleation energy consumption facilitated by the heterogeneous structure. For example, introducing Nb nanowires into Ni−Ti alloys results in a notable reduction in stress hysteresis compared to typical Ni−Ti SMAs. Moreover, the nanocomposite materials obtained through additive manufacturing of Ni−Ti, feature Ni-rich intermetallic compounds dispersed within a binary alloy matrix, also demonstrate superelasticity with minimal hysteresis [17]. However, it is noteworthy that the critical stress for stress-induced martensitic phase transformation (σ_{SIM}) in these alloys remains highly sensitive to temperature. The critical stress required to induce a martensitic transformation increases with the increase of temperature due to the enhanced stability of the parent phase relative to the martensite. For practical applications of superelasticity, it is essential that the stress response remains insensitive to temperature variations. The adjustable temperature dependence of the critical stress enables engineers and scientists to design structures and components with desired properties. Recently, the near-constant critical stress temperature dependence has been observed in Fe−Mn−Al−Cr−Ni single crystals [18]. However, the preparation of single crystals is challenging, and these alloys exhibit relatively low recoverable strain (~2%) and significant stress hysteresis. Addressing the issue of reducing stress hysteresis while increasing the recoverable strain and improving temperature dependence remains a scientific challenge that warrants further in-depth research. High-entropy alloys (HEAs) are typically defined as alloys that contain a minimum of five principal elements, each with a concentration ranging between 5 and 35 at.% [19−21]. HEAs have attracted much attention due to its unique microstructure and unexpected properties [22−24]. Recently, the concept of HEA has been introduced into SMAs, leading to the development of a series of high-entropy shape memory alloys (HESMAs), such as $(TiZrHf)_{50}(NiCoCu)_{50}$ [25], $FeNi_{27.5}Co_{16.5}Al_{10}Ta_{2.2}B_{0.04}$ [26], and $NiCuTiHf_{0.6}Zr_{0.4}$ [27]. Compared to traditional SMAs, HESMAs exhibit significant improvements, including enhanced martensitic phase transition temperatures [28,29], high strength, excellent high-temperature phase stability, wide temperature range superelasticity, and high damping properties. However, these alloys still face challenges such as sensitive temperature dependence, low recoverable strain, and large stress hysteresis.

Based on the Ni−Mn−Ti SMAs system, we innovatively introduced the design concept of HEAs and successfully prepared a novel $Ni_{35}Mn_{25}Ti_{15}Fe_{15}Co_{10}$ multi-principal element alloy using arc melting technology. For characterization methods, we systematically analyzed the phase composition characteristics of the alloy through X-ray diffraction (XRD) and transmission electron microscopy (TEM) techniques, while innovatively establishing a simplified elastocaloric testing method to replace the complex in-situ high-energy X-ray diffraction technique (HE-XRD) for phase transformation behavior research. The alloy demonstrated significantly enhanced strength through lattice distortion induced by the high-entropy effect, and exhibited superior recoverable elastic strain and stable stress−temperature dependence over a wide temperature range based on weak first-order martensitic transformation, showing great application potential for extreme environments with severe temperature fluctuations such as outer space.

2 Experimental

Polycrystalline $Ni_{35}Mn_{25}Ti_{15}Fe_{15}Co_{10}$ (at.%) alloy ingots were prepared via arc melting in an argon atmosphere with high-purity Ni, Mn, Ti, Fe, and Co. The alloy was denoted as Ni35 based on the molar fraction of Ni in the nominal composition. The heat-treated ingots were processed in a vacuum quartz tube furnace through annealing at 1223 K for 24 h followed by rapid water quenching (WQ). Samples with various sizes were sectioned from the central region of ingots using a spark wire cutting machine

for subsequent experiments.

The microstructure and chemical composition of the alloy were characterized by means of scanning electron microscopy (SEM, JSM−7001F) equipped with energy dispersive spectrometry (EDS). Selected area electron diffraction patterns were observed utilizing a transmission electron microscope (TEM, JEM−2100F) to further determine the room-temperature crystal structure. The crystal structure was examined using an X-ray diffractometer (XRD, Rigaku SMARTLAB 9) with Cu K_α radiation. Phase transformation behavior was analyzed by means of differential scanning calorimetry (DSC, TA-Q100) in nitrogen atmosphere with cooling/heating rate of 10 K/min.

Compression tests were conducted on 3 mm × 4 mm × 6 mm specimens across a temperature range from 113 to 433 K. To ensure the reliability of the results, three parallel experiments were performed using the same mechanical testing machine (AG-XPlus 50 kN). A K-type thermocouple was attached to the surface of the bulk sample, and a paperless temperature recorder (KSB01A0B) was used to monitor the adiabatic temperature changes on the surface of the sample under the applied stress field. Furthermore, the thermomagnetic behavior was investigated using an MPMS−3 superconducting quantum interference device magnetometer (SQUID), applying a small field of 0.05 T with cooling/heating rate of 10 K/min.

3 Results

3.1 Microstructure and phase identification

Figure 1 presents SEM images illustrating the microstructure of the as-cast and annealed polycrystalline Ni35 alloys. The as-cast Ni35 alloy exhibits a eutectic lamellar microstructure (highlighted by yellow circle in Fig. 1(a)), characterized by a distinct contrast between the matrix lamellae (dark) and the precipitate lamellae (light). The eutectic microstructure of the Ni35 alloy exhibits a fine and uniform distribution of the precipitates. However, the lamellar structure of the eutectic microstructure is disrupted in annealed Ni35 alloy, as shown in Fig. 1(b). The heat-treated alloy demonstrates a significant increase in the size of precipitates, evolving from the lamellar structure observed in the as-cast alloy to a considerably coarser columnar and spherical morphology.

Figure 1(c) depicts a secondary electron micrograph of the as-cast Ni35 alloy, and Figs. 1(d−h) show the elemental mapping images for Ni, Mn, Ti, Fe and Co, respectively. It can be seen that the matrix

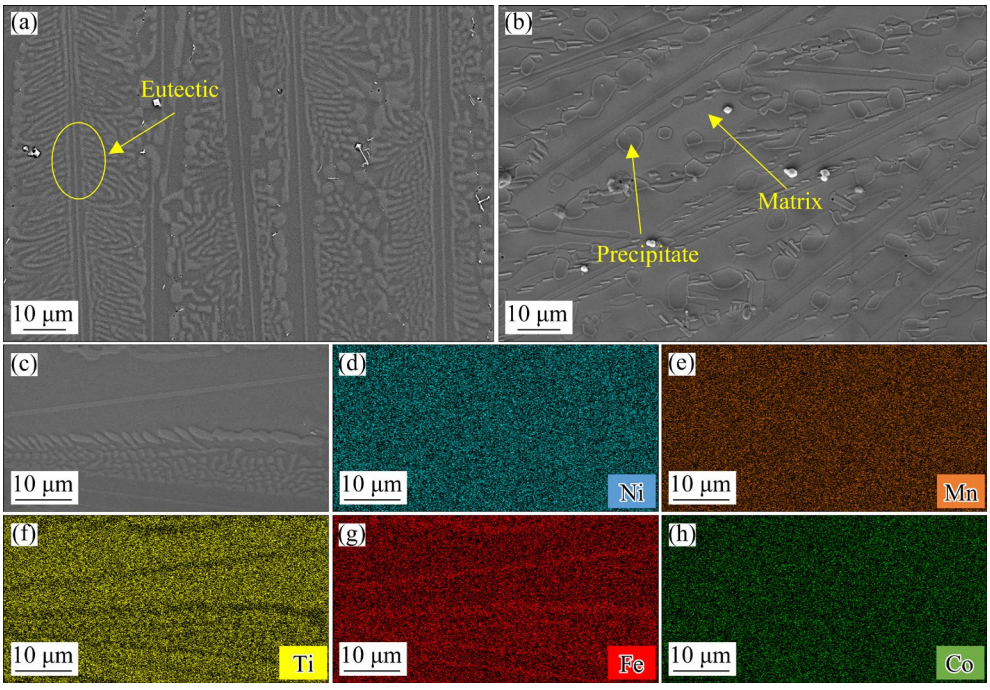

Fig. 1 SEM images and EDS elemental analysis results of Ni35 alloys: (a) Micrograph of as-cast Ni35 alloy; (b) Micrograph of heat-treated Ni35 alloy; (c) Secondary electron micrograph of as-cast Ni35; (d−h) EDS mappings for Ni, Mn, Ti, Fe and Co, respectively

exhibits a higher Fe content and a lower Ti content compared to the γ' phase. The differences in Ni, Mn and Co contents between two phases are relatively minor. Compositional analysis of the matrix and the precipitate was determined by EDS, with summarized results presented in Table 1. It can be seen that the precipitate consists of higher Fe content and lower Ti content compared with the matrix, and the content of other elements is basically the same.

Figure 2 presents TEM images of the as-cast Ni35 alloy. Figure 2(a) shows a bright-field TEM image of the eutectic structure. Austenite usually exists in B2 or $L2_1$ structural forms, which can be identified by TEM from specific zone axes. In Fig. 2(b), superlattice diffraction spots corresponding to the (001) plane of the B2 structure are observed, while no superlattice diffraction spots corresponding to the $L2_1$ structure (110) are detected. This indicates that the austenite in this alloy possesses a B2 structure. In Fig. 2(c), superlattice diffraction spots corresponding to the (100) plane of γ' are observed. The γ' lamellae, which are in the bright contrast, are approximately 350 nm in thickness and about 500 nm in spacing between them. Compared to B2 (BCC structure), γ' (FCC structure) possesses more slip systems, facilitating dislocation motion. Therefore, γ' phase exhibits lower hardness but enhanced plasticity, thereby making a greater contribution to the alloy's overall plasticity.

3.2 Crystal structure

Figure 3 shows the XRD patterns of the as-cast alloys with different pre-strains (ε) at room temperature. The alloy exhibits a mixed structure comprising the B2 austenite and FCC γ' phase. As the deformation increases, the peak intensities of γ'(200) and γ'(220) noticeably diminish, while the peak intensity of B2(220) strengthens. Typically, shape memory alloys retain residual martensite after deformation, but characteristic peaks of martensite are not found in the XRD patterns of the deformed Ni35 alloy. This phenomenon indicates that the stress-induced martensite can completely reverse back to austenite after unloading, and it may be related to the eutectic microstructure in the as-cast Ni35 alloy.

3.3 Mechanical properties and cyclability

The mechanical properties of the Ni35 alloys are shown in Fig. 4. In Fig. 4(a), the compressive engineering stress−strain curves at a strain rate of $2.78\times10^{-4}\ s^{-1}$ for the Ni35 alloy in both as-cast and heat-treated states at room temperature are depicted. It can be observed that the as-cast alloy exhibits yielding at approximately 5% strain, whereas the heat-treated alloy yields at around 3% strain. The yielding point (indicated by arrow) of the as-cast Ni35 alloy may correspond to stress-induced martensite transformation, as this alloy predominantly exists in a eutectic state with B2 austenite and γ' phase at room temperature. Notably, compared to other SMAs, this alloy demonstrates an exceptionally high critical stress for stress-induced martensitic phase transformation. Conversely, no such yielding behavior was observed in the heat-treated alloy without the eutectic structure, resulting in weakened strength and ductility of the alloy.

Table 1 Chemical compositions of matrix and precipitates in Ni35 alloy (at.%)

Matrix					Precipitate				
Ni	Mn	Ti	Fe	Co	Ni	Mn	Ti	Fe	Co
34.29	24.86	17.25	13.27	10.33	33.71	25.95	10.87	19.98	9.50

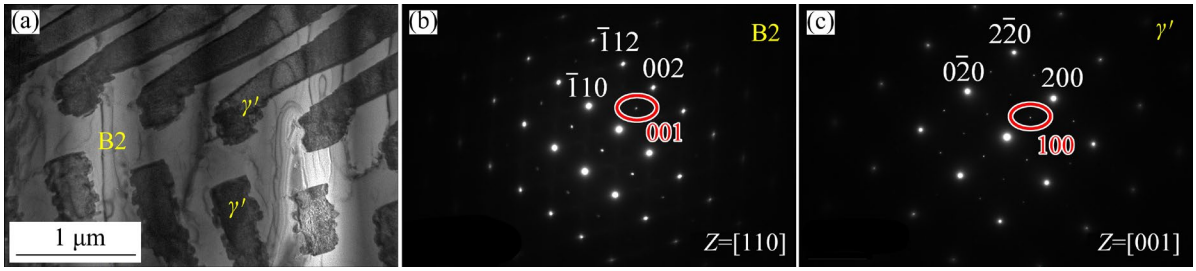

Fig. 2 TEM images of as-cast Ni35 alloy: (a) Bright-field TEM micrograph; (b) Selected area electron diffraction pattern of B2 phase; (c) Selected area electron diffraction pattern of FCC γ' phase

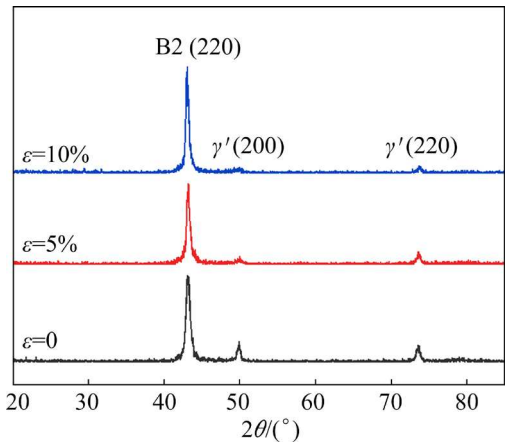

Fig. 3 XRD patterns of as-cast Ni35 alloy with different pre-strains

After heat treatment, the compressive ductility and strength of the alloy decrease from 20.85 % and 1875.01 MPa in the as-cast state to 12.07% and 1309.14 MPa, respectively. The phenomenon can be explained by microstructural coarsening and the weakening of the high-entropy effect. As shown in Fig. 1(a), after heat treatment, the lamellar structures of the γ' phases in the alloy coarsen or even spheroidize, leading to the disintegration of the lamellar network. As a result, the microstructure can no longer effectively hinder dislocation motion, resulting in a degradation of mechanical properties.

Additionally, heat treatment has a significant impact on the high-entropy effect in HEAs. During heat treatment, the intensified thermal motion of elements may cause elemental segregation, phase separation, or increased degree of atomic order of the alloy. This weakens the high-entropy effect, further resulting in declined mechanical properties. To summarize, heat treatment causes a deterioration in the mechanical performance of the alloy.

Figure 4(b) illustrates a few selected loading−unloading cycles of the as-cast Ni35 alloy, and all subjected to a stress of 1600 MPa. In the first cycle, the as-cast alloy exhibits a deformation strain of 11.9% and a residual strain of 3.7%, resulting in a recovered strain of about 8.2%. Subsequently, the loading−unloading cycles show quasi-linear stress−strain loops with minimal hysteresis after a few initial cycles. The excellent superelastic behavior is primarily attributed to the superelastic training effect. On the one hand, dislocations and residual martensite formed in the first cycle are positioned favorably, providing conducive internal stress for the nucleation of martensite and subsequent phase transformation [30]. On the other hand, the initially formed dislocations impede further generation of dislocations during subsequent phase transformation cycles, facilitating complete reversibility of stress-induced martensitic phase transformation and reducing energy dissipation in subsequent cycles [30,31]. The stress hysteresis, recoverable strain and apparent Young's modulus of the as-cast Ni35 alloy are presented in Fig. 4(c) as functions of deformation cycles. The stress hysteresis exhibits a rapid decline from 55.27 to 4.99 MPa within the initial two cycles, eventually stabilizing at approximately 1.40 MPa with continued cycling. The recoverable strain decreases slightly from 8.21% to 8.17% with deformation cycling. The

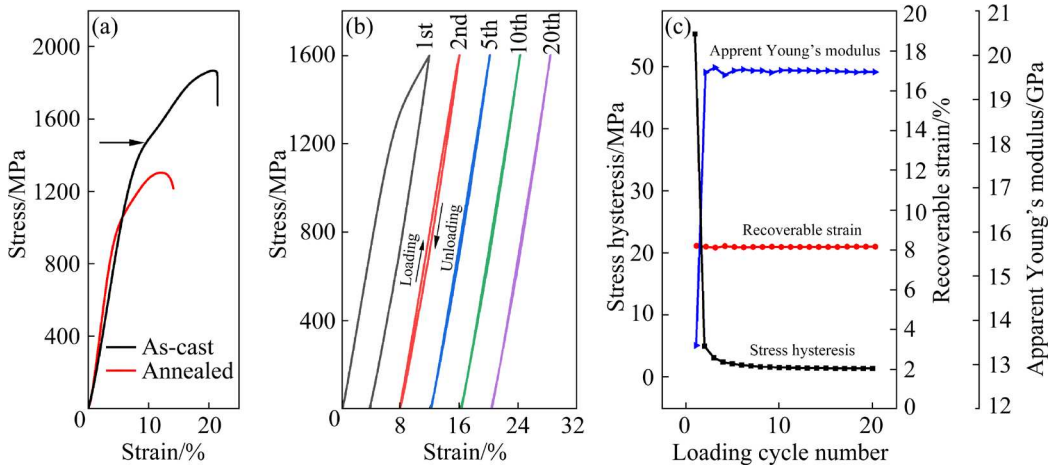

Fig. 4 Mechanical properties of Ni35 alloys: (a) Compressive engineering stress−strain curves of Ni35 alloys at 2.78×10^{-4} s^{-1}; (b) Compressive deformation cycling properties of as-cast Ni35 alloy; (c) Stress hysteresis, recoverable strain and apparent Young's modulus during deformation cycling of as-cast Ni35 alloy

apparent Young's modulus increases rapidly from 13.43 to 19.62 GPa in the initial two cycles and stabilizes at approximately 19.62 GPa with further cycling. Such a low Young's modulus, which contributes to a high recoverable strain, is atypical for metallic materials and suggests the occurrence of SIMT during the deformation process. This behavior is indicative of "pseudoelasticity".

3.4 Martensitic transformation during deformation process

Studying the dynamic evolution of the crystal structure of alloys exhibiting narrow hysteresis superelasticity during the loading−unloading processes often involves the utilization of in-situ characterization techniques with synchrotron radiation. However, due to the equipment limitation, in this work, we employed in-situ HE-XRD measurement to study the phase transformation during the loading−unloading processes. Martensitic phase transformation in SMAs typically constitutes a first-order phase transition, which can result in significant heat changes. Based on this principle, it is possible to ascertain whether martensitic transformation occurs during the loading−unloading processes by detecting thermal effects. In this work, we employed elastocaloric experiments instead of in-situ HE-XRD measurement to qualitatively investigate the phase transitions of the alloy during the loading−unloading processes. To verify the pseudo-elasticity of the deformation process, an elastocaloric measurement was conducted during the loading−unloading process of the as-cast Ni35 alloy at a strain rate of 5.6×10^{-2} s^{-1}.

Figures 5(a) and (b) illustrate the thermodynamic temperature changes (ΔT_{ad}) of the as-cast Ni35 alloy during the loading−unloading processes at a strain from 1% to 13%. When the alloy was subjected to cyclic loading at a strain of 1%, the ΔT_{ad} was very small, approximately only 0.1 K. As the strain increased from 1% to 5%, the ΔT_{ad} of the alloy increased from 0.1 to 0.7 K during the loading process, as depicted in Fig. 5(c). These slight ΔT_{ad} values often arise from elastic deformation or continuous phase transformation. It is noteworthy that during cyclic testing with a strain of 6%, the ΔT_{ad}

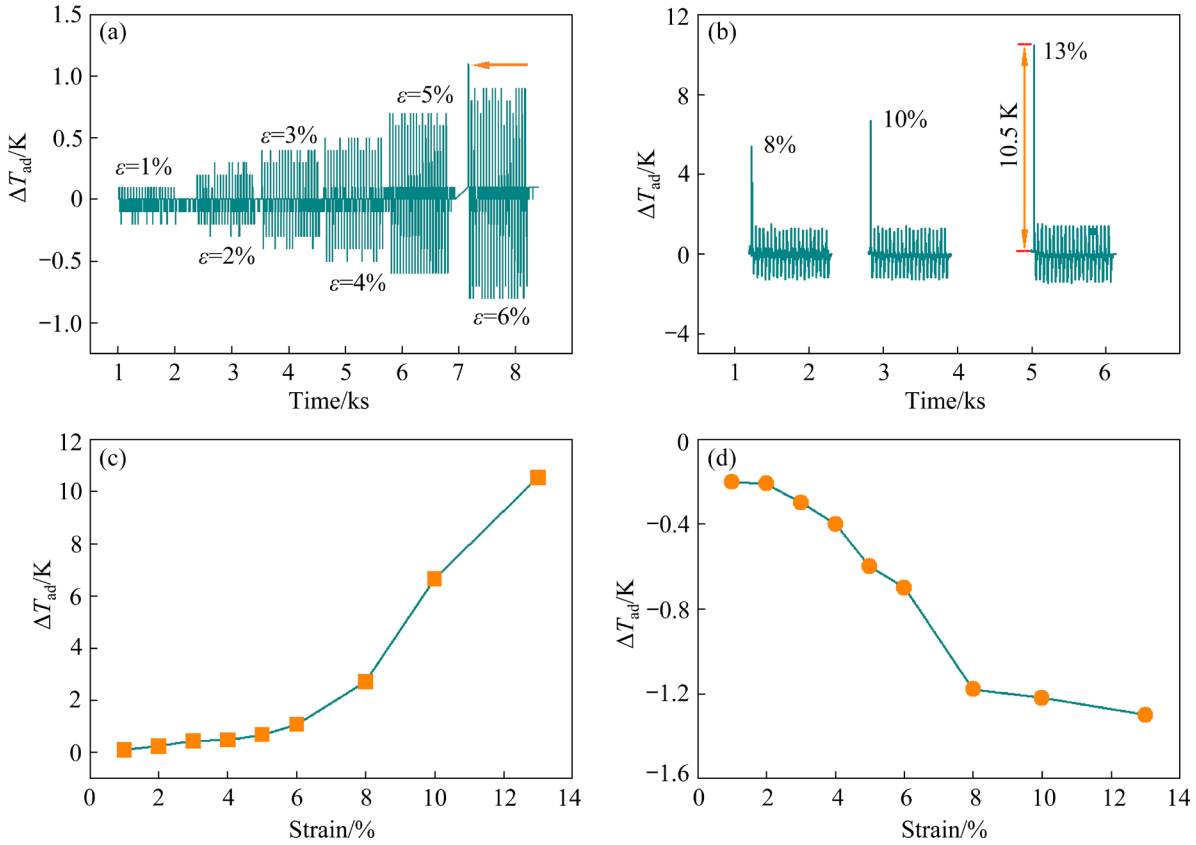

Fig. 5 Elastocaloric effect of as-cast Ni35 alloy: (a) Time dependence of temperature change at strains of 1%−6%; (b) Time dependence of temperature change at strains of 8%−13%; (c) The first exothermic temperature change at different strains; (d) The 20th endothermic temperature change at different strains

in the first cycle of the alloy was significantly higher than that in the subsequent 19 cycles (highlighted by the orange arrow in Fig. 5(a)). Similar phenomena were observed during cyclic testing of the as-cast Ni35 alloy at strains of 8%, 10%, and 13%, as shown in Fig. 5(b). Moreover, as the strain increased, the first exothermic temperature change in the cyclic tests also increased. When the strain increased from 8% to 13%, the first exothermic temperature change indicated a first-order martensitic phase transformation in the as-cast Ni35 alloy during the deformation from 8% to 13%. However, the ΔT_{ad} in the subsequent 19 cycles exhibits only a slight increasing trend with increasing strain, as shown in Fig. 5(b).

To ensure the accuracy of temperature measurements, a K-type thermocouple was attached to the surface of the bulk sample, allowing real-time monitoring of temperature changes with high precision. During the experiments, the thermal response of the alloy exhibited noticeable asymmetry during the first loading and unloading cycle. This phenomenon may appear unusual at first glance, but it is fundamentally related to the phase transformation behavior and hysteresis effects. Specifically, during loading, stress-induced martensitic transformation occurs, leading to significant heat release and a corresponding temperature rise.

Conversely, during unloading, the reverse transformation absorbs heat, causing a temperature drop. However, due to the hysteresis effect, energy dissipation during the phase transformation process often results in incomplete or delayed reverse transformation, leading to the observed asymmetry in the curves. This hysteresis between loading and unloading is a characteristic feature of shape memory alloys, primarily caused by energy dissipation during phase transformation, which is also the key factor contributing to the asymmetry in the elastocaloric experimental results.

Figures 5(a) and (b) indicate that during cyclic testing within a strain range of 1%−5%, the as-cast Ni35 alloy undergoes minimal heat change, suggesting the absence of a first-order phase transformation occurred during this stage. However, with cyclic testing within a strain range of 6%−13%, a significant heat change was observed only during the first cycle, indicating that a first-order martensitic transformation occurred during the initial cycle.

Conventionally, alloys generate heat due to internal friction during elastic deformation, resulting in heat generation during both loading and unloading processes. However, in this experiment, exothermic behavior was not detected during unloading in the elastic stage of the as-cast Ni35 alloy. Instead, endothermic behaviors were observed, as shown in Figs. 5(a, b, d). Therefore, phase transformation must occur during the deformation process. However, it may no longer be a strong first-order phase transition, but rather a weak first-order martensitic phase transformation or even a continuous phase transition. These alloys exhibited endothermal effects during 20 cycles, indicating the stability of the weak first-order martensite transformation. Figure 5(d) illustrates the endothermal ΔT_{ad} at the 20th unloading stage under different strains.

3.5 Superelastic behavior

Distinguished from the superelasticity of traditional SMAs, the novel high-entropy $Ni_{35}Mn_{25}Ti_{15}Fe_{15}Co_{10}$ alloy exhibits quasi-linear superelasticity. Figure 6 illustrates the compressive superelastic stress−strain curves at a strain rate of 1.39×10^{-3} s^{-1}. An ultralarge quasi-linear superelasticity of 6% strain can be achieved under a stress field of 1176 MPa in the as-cast Ni35 alloy, as shown in Fig. 6(a). Furthermore, when the strain decreases to 5% under a stress field of 1010 MPa, the as-cast Ni35 alloy displays linear superelasticity with almost zero stress hysteresis. However, compared to the as-cast alloy Ni35, the annealed Ni35 alloy exhibits a degradation in quasi-linear superelasticity. Specifically, the annealed alloy demonstrates a quasi-linear superelasticity of 5% strain under a stress field of 912 MPa and a linear superelasticity of 4% strain under a stress field of 720 MPa, as shown in Fig. 6(a).

Figure 6(b) displays a few selected stress−strain curves of the as-cast Ni35 alloy with a 5% strain during 12010 cycles. Remarkably, after 12010 cycles, no significant changes were observed in the hysteresis or the stress corresponding to a 5% strain for the alloy, indicating its excellent cyclic stability. The cyclic stability of this novel $Ni_{35}Mn_{25}Ti_{15}Fe_{15}Co_{10}$ high-entropy alloy is attributed to its nearly-zero hysteresis. In traditional SMAs, the stress-induced phase transformation between the parent phase and the martensitic phase requires the provision of driving forces. Moreover, frictional

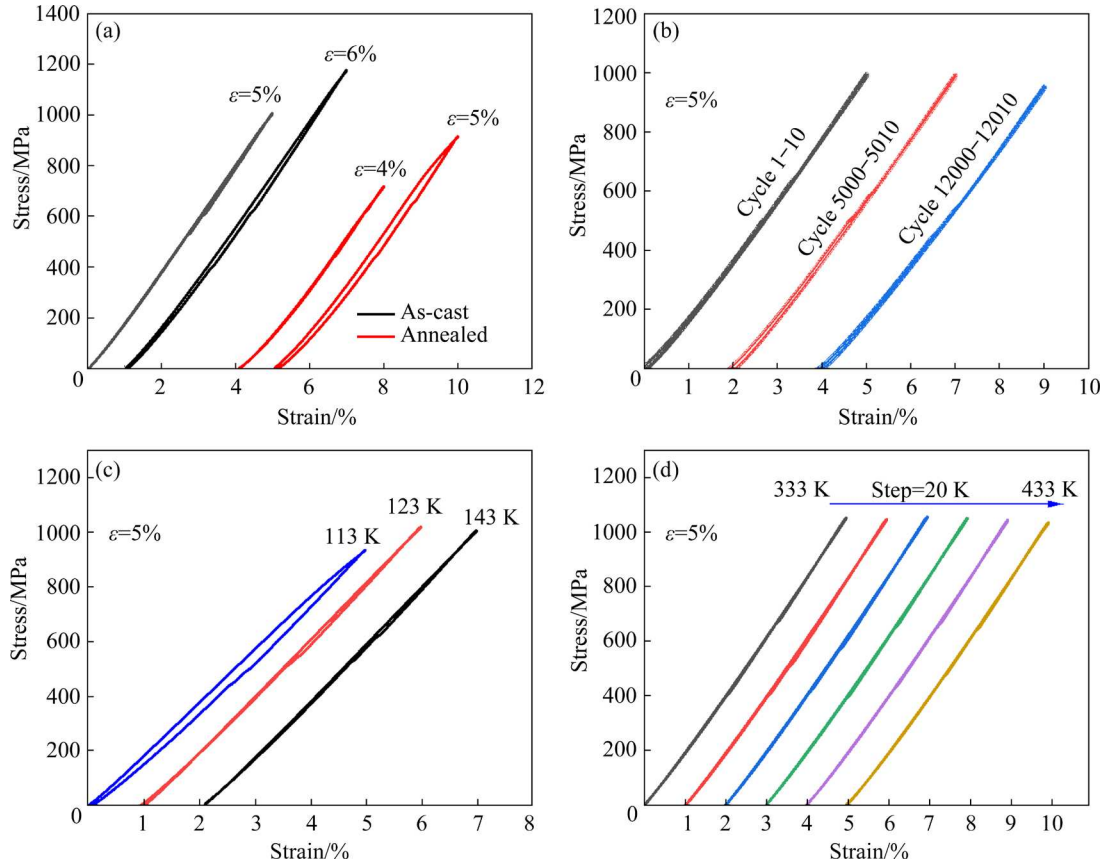

Fig. 6 Superelastic stress–strain curves of Ni35 alloys: (a) Comparison of superelasticity between as-cast and annealed Ni35 alloys; (b) Cyclic stability of as-cast alloy; (c, d) Superelastic stress–strain curves of as-cast alloy at different temperatures

resistance arising from the migration of phase interfaces between the parent phase and the new phase, interactions between martensite variants, and defects inevitably lead to energy dissipation [20], manifesting in the form of stress hysteresis. Therefore, stress hysteresis is inherent in superelasticity resulting from thermodynamically first-order martensitic transformation. Additionally, during cyclic loading, the dislocations and residual martensite accumulate within the alloy, further reducing the functional cyclic stability and service life of the alloy.

Figures 6(c, d) display the compressive stress–strain response at different temperatures. In the as-cast Ni35 alloy, an almost zero temperature dependence of superelasticity, with a strain of 5% and a stress of approximately 1050 MPa, is obtained from 123 to 433 K. However, when the temperature drops to 113 K, the stress corresponding to a 5% strain of the alloy suddenly decreases, with the stress decreasing from 1025 MPa at 123 K to 938 MPa at 113 K. Such a low temperature dependence of superelasticity within a wide temperature span is rare in polycrystalline alloys. Previously, almost zero temperature dependence of superelasticity was also observed in Fe−Mn−Al−Cr−Ni single crystal, but the strain in that alloy was less than 2%, and there was obvious stress hysteresis in superelasticity [18].

4 Discussion

4.1 Weak first-order martensitic transformation

The Ni35 alloy features a distinctive eutectic microstructure characterized by alternating eutectic lamellae, which creates numerous phase boundaries. Dislocations are frequently observed at these phase interfaces, serving as pre-existing high nucleation sites [32]. These defects play a crucial role in lowering or even completely suppressing the energy barriers for martensite nucleation [33]. Furthermore, new dislocations are generated during the loading process. Both the inherent dislocations in the alloy and those formed during loading can serve as nucleation sites, thereby reducing the energy barriers

for martensite during the forward transformation and for austenite during the reverse transformation [21]. This mechanism enables the alloy to exhibit superelasticity with minimal hysteresis. The abundance of dislocations is correlated with lower energy barriers, which is favorable for phase transformation. When the dislocations reach a certain quantity, martensitic transformation may change from a strong first-order transformation to a weak first-order or even a continuous transformation.

4.2 Linear superelasticity

The quasi-linear recovery behavior arises from the efficient load transfer mechanism between the non-transformed γ' phase and the transformed phase, and has been observed in other alloys [34−36]. As depicted in Fig. 6(a), the effective modulus of the as-cast Ni35 alloy (~20.2 GPa) is higher than that of the heat-treated Ni35 alloy (~18.2 GPa), underscoring the significant influence of the non-transformed γ' phase in mechanical response. During the transformation of austenite to martensite, the γ' phase continues to carry the load elastically, contributing to the overall quasi-linear behavior. In eutectic alloys, the closely alternating arrangement of two-phase lamellae facilitates efficient load transmission. The precipitates play a pivotal role in guiding the transformation process through elastic interactions with the austenite, thus mitigating the multiple instabilities commonly associated with traditional nucleation and rapid growth. This reduction in energy dissipation and interfacial friction enhances the superelastic behavior of the as-cast Ni35 alloy, whereas in the heat-treated Ni35 alloy, the disruption of the eutectic microstructure diminishes load transmission between the two phases, which leads to a decline in linear superelasticity, as illustrated in Fig. 6(a).

In traditional shape memory alloys, the onset of first-order martensitic transformation typically occurs rapidly once the applied load surpasses the critical stress threshold. This results in a nonlinear stress−strain curve characterized by a stress plateau, which can significantly affect the control precision of shape memory alloys in certain applications. In this work, according to the thermoelastic experiment, the as-cast Ni35 alloy undergoes first-order martensitic transformation only under large deformation (ε>5%). Notably, the weak first-order martensitic transformation does not occur in an "avalanche" manner, thus no stress plateau appears in the stress−strain curve. This unique behavior endows the alloy exhibiting linear superelasticity. The linear superelasticity is attributed to the synergistic effects of load transfer between eutectic phases and the absence of first-order martensitic transformation under small deformations. This distinctive combination enables the alloy to achieve a linear stress−strain response, thereby enhancing its suitability for precise control applications.

4.3 First-order martensitic transformation

According to the aforementioned thermoelastic experiments, it is evident that the alloy undergoes stress-induced first-order martensitic transformation when the strain reaches a critical value (ε_c). When the strain is below this value, the applied stress induces a weak first-order martensitic transformation. The alloy exhibits a linear superelasticity of 5%, but during cyclic testing at 1600 MPa, the linear superelasticity reaches as high as about 8.2%. This phenomenon may be attributed to the existence of ε_c in this alloy. Beyond the ε_c, the alloy exhibits significant superelasticity.

At smaller strains, a fraction of the austenite in the alloy undergoes stress-induced weak first-order martensitic transformation near dislocations. As the strain increases, the proportion of austenite undergoing phase transformation also increases. When the strain exceeds the ε_c, the load surpasses the critical stress threshold, triggering first-order martensitic transformation. Austenite that did not transform begins to undergo this first-order martensitic transformation.

Furthermore, at larger strains, a significant number of dislocations are generated in the alloy, providing nucleation sites for martensite and austenite, reducing the energy barrier. This facilitates the occurrence of the weak first-order martensitic transformation during subsequent cyclic loading processes. This is the reason why, during cyclic loading at large strains, the alloy undergoes first-order martensitic transformation and generates a substantial amount of heat only during the initial loading stage.

To further confirm martensitic transformation in the as-cast Ni35 alloy, TEM characterization and XRD analysis were conducted, as shown in Fig. 7. The as-cast Ni35 alloy was subjected to 10% pre-strain treatment prior to TEM characterization, and

the bright-field TEM image is illustrated in Fig. 7(a). Martensite is clearly observed at the interface between the austenite and γ' phase in Fig. 7(a), which is residual martensite generated due to severe deformation. Additionally, a large number of dislocations can be observed in the austenite, which can serve as nucleation sites for weak first-order phase transformation. This promotes the occurrence of weak first-order phase transformation while impeding the reverse martensitic transformation of martensite to austenite upon unloading (first-order phase transformation), thereby resulting in residual martensite in the alloy.

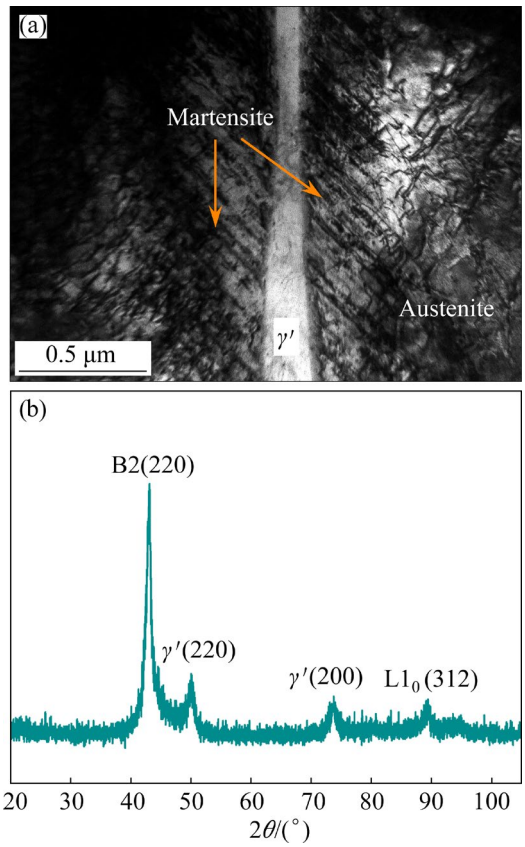

Fig. 7 Characterization results of martensite in as-cast Ni35 alloy: (a) Bright field (TEM) image; (b) XRD pattern

In the XRD analysis described above (Fig. 3), no characteristic peaks of martensite were detected in the as-cast Ni35 alloy pre-strained to 10%, which may be attributed to the limited presence of residual martensite in the alloy. With increased deformation, more dislocations are formed in the alloy, effectively hindering the first-order phase transformation from martensite to austenite upon unloading, resulting in a higher presence of residual martensite in the alloy. Consequently, it becomes easier to detect martensite in XRD measurements. We ground the as-cast Ni35 alloy into powder for XRD testing and detected the characteristic peak of $L1_0(312)$, as shown in Fig. 7(b). The characteristic peak has also been detected in another paper [37]. Hence, there exists martensitic phase transformation in the Ni35 alloy.

4.4 Low temperature dependence

The temperature-dependent nature of super-elasticity based on the first-order martensitic transformation imposes significant limitations on the practical applications of SMAs, especially in precision instruments where thermal expansion must be minimized. Moreover, the Ni35 alloy exhibits diverse crystal orientations, which complicates subsequent analysis due to the dependency of critical stress on temperature ($\mathrm{d}\sigma/\mathrm{d}T$) on the specific orientation. This behavior can be expressed through the Clausius−Clapeyron relationship in Eq. (1):

$$\frac{\mathrm{d}\sigma}{\mathrm{d}T}=-\frac{\Delta S}{\varepsilon V} \tag{1}$$

where T represents the temperature; ΔS is the entropy change during martensitic transformation; ε is the transformation strain, which depends on the orientation; V is the molar volume. Because the ΔS and V are orientation-independent during martensitic transformation, the $\mathrm{d}\sigma/\mathrm{d}T$ is inversely proportional to ε. As shown in Fig. 8, the magnetization−temperature (M−T) curve of the as-cast Ni35 alloy indicates the absence of first-order martensitic transformation in the temperature range from 50 to 375 K. Therefore, within this temperature range, the entropy of the alloy remains nearly constant, resulting in the entropy change close to zero, and an extremely low temperature dependence ($\mathrm{d}\sigma/dT$) of the alloy.

The Ni35 alloy demonstrates exceptional suitability for applications spanning a broad temperature range (113−433 K), making it ideal for structural damping and space research. As society's interest in space exploration continues to grow, the demand for advanced materials is also on the rise. The exploration of the Moon, with its extreme day-night temperature fluctuations (ranging from 400 to 100 K), and Mars, with temperature variations from 290 to 120 K, necessitates materials capable of operating under such harsh conditions. The Ni35 alloy, with its low temperature dependence over a wide range, emerges as a highly promising candidate for use in some extreme temperature conditions.

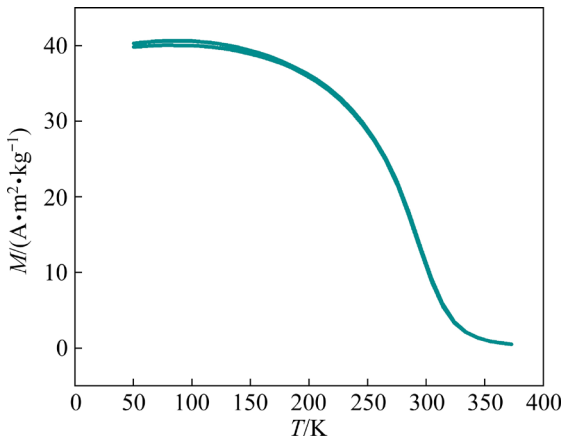

Fig. 8 M−T curve of as-cast Ni35 alloy under small magnetic field intensity of 0.05 T

5 Conclusions

(1) The as-cast Ni35 alloy presents a eutectic microstructure of B2 austenite and FCC γ' phases, eliminated by heat treatment (1223 K, 24 h, WQ). The alternating phase arrangement in the eutectic structure creates numerous interfaces, essential for enabling weak first-order martensitic transformation.

(2) The as-cast Ni35 alloy with nearly-full eutectic microstructure achieves optimal mechanical properties, including a compressive strength of 1875.01 MPa, ductility of 20.85%, and stable cyclability. This demonstrates a low apparent Young's modulus (19.62 GPa), slim stress hysteresis (1.40 MPa), and ultralarge linear superelasticity (8.2%), attributed to its eutectic structure and weak first-order martensitic transformation.

(3) The alloy exhibits superelastic behavior with 5% strain from 113 to 433 K, showing nearly zero temperature dependence and minimal hysteresis between 123 and 433 K. This low temperature dependency arises from the inability of temperature alone to induce martensitic phase transformation in the alloy.

(4) During elastocaloric cycling experiments, the alloy releases substantial heat during initial large deformations, driven by strong first-order martensitic transformation.

CRediT authorship contribution statement

Ke-liang GUO: Investigation, Methodology, Data curation, Funding, Writing − Original draft; **Yu ZHANG:** Supervision, Validation; **Jiang-long GU:** Data curation; **Jing BAI:** Supervision, Formal analysis, Project administration, Funding acquisition, Writing − Review & editing; **Dan LIU:** Investigation; **Nicola MORLEY:** Resources; **Qing-shuang MA:** Software; **Qiu-zhi GAO:** Investigation; **Liang ZUO:** Supervision, Resources.

Declaration of competing interest

The authors declare that they have no known competing financial interests or personal relationships that could have appeared to influence the work reported in this paper.

Acknowledgments

This work was financially supported by the National Natural Science Foundation of China (No. 51771044), the Performance Subsidy Fund for Key Laboratory of Dielectric and Electrolyte Functional Material of Hebei Province, China (No. 22567627H), the 2024 Hebei Provincial Doctoral Candidate Innovation Ability Training Funding Project, China (No. CXZZBS2023179), the Hebei Central Government-Guided Local Science & Technology Development Fund Project, China (No. 246Z1026G), and the Ministry of Education's "Chunhui Program" Collaborative Research Project, China (No. HZKY20220244).

References

[1] JANI J M, LRARY M, SUBIC A, GIBSON M A. A review of shape memory alloy research, applications and opportunities [J]. Materials & Design, 2014, 56: 1078−1113.

[2] HARTL D J, LAGOUDAS D C. Aerospace applications of shape memory alloys [J]. Proceedings of the Institution of Mechanical Engineers (Part G): Journal of Aerospace Engineering, 2007, 221(4): 535−552.

[3] HAO Shi-jie, CUI Li-shan, JIANG Da-qing, HAN Xiao-dong, REN Yang, JIANG Jiang, LIU Yi-nong, MA Sheng-chen, WANG Yan-dong, LI Yan, REN Xiao-bing, DING Xiang-dong, WANG Shan, YU Cun, SHI Xiso-bin, DU Min-shu, YANG Feng, ZHENG Yan-jun, ZHANG Ze, LI Xiao-dong, BROWN D E, LI Ju. A transforming metal nanocomposite with large elastic strain, low modulus, and high strength [J]. Science, 2013, 339(6124): 1191−1194.

[4] TIAN Lin, CHENG Yong-qiang, SHAN Zhi-wei, LI Ju, WANG Cheng-cai, HAN Xiao-dong, SUN Jun, MA E. Approaching the ideal elastic limit of metallic glasses [J]. Nature Communications, 2012, 3: 609.

[5] ZHANG Ru-fan, WEN Qian, QIAN Wen-zhong, SU Dang-sheng, ZHANG Qiang, WEI Fei. Superstrong ultralong carbon nanotubes for mechanical energy storage [J]. Advanced Materials, 2011, 23(30): 3387−3391.

[6] GHADIMI A H, FEDOROV S A, ENGELSEN N J, BEREYHI M J, SCHILLING R, WILSON D J, KIPPENBERG T J. Elastic strain engineering for ultralow mechanical dissipation [J]. Science, 2018, 360(6390): 764−768.

[7] YANG Sheng-xue, CHEN Yu-jia, JIANG Cheng-bao. Strain engineering of two-dimensional materials: Methods, properties, and applications [J]. InfoMat, 2021, 3(4): 397−420.

[8] OMORI T, ANDO K, OKANO M, XU Xiao, TANAKA Y, OHNUMA I, KAINUMA R, ISHIDA K. Superelastic effect in polycrystalline ferrous alloys [J]. Science, 2011, 333(6038): 68−71.

[9] OTSUKA K, REN Xiao-bing. Physical metallurgy of Ti−Ni-based shape memory alloys [J]. Progress in Materials Science, 2005, 50(5): 511−678.

[10] OTSUKA K, WAYMAN C M, NAKAI K, SAKAMOTO H, SHIMIZU K. Superelasticity effects and stress-induced martensitic transformations in Cu−Al−Ni alloys [J]. Acta Metallurgica, 1976, 24(3): 207−226.

[11] CHEN Hai-yang, WANG Yan-dong, NIE Zhi-hua, LI Run-guang, CONG Dao-yong, LIU Wen-jun, YE Feng, LIU Yu-zi, CAO Pei-yu, TIAN Fu-yang, SHEN Xi, YU Ri-cheng, VITOS L, ZHANG Ming-he, LI Shi-lei, ZHANG Xiao-yi, ZHENG Hong, MITCHELL J F, REN Yang. Unprecedented non-hysteretic superelasticity of [001]-oriented NiCoFeGa single crystals [J]. Nature Materials, 2020, 19(7): 712−718.

[12] ZHANG Zhen, DING Xiang-dong, SUN Jun, SUZUKI T, LOOKMAN T, OTSUKA K, REN Xiao-bing. Nonhysteretic superelasticity of shape memory alloys at the nanoscale [J]. Physical Review Letters, 2013, 111(14): 145701.

[13] GAO Yi-ping, CASALENA L, BOWERS M L, NOEBE R D, MILLS M J, WANG Yuan-yuan. An origin of functional fatigue of shape memory alloys [J]. Acta Materialia, 2017, 126: 389−400.

[14] HSU W N, POLATIDIS E, SMID M, van PETEGEM S V, CASATI N, van SWYGENHOVEN H. Deformation and degradation of superelastic NiTi under multiaxial loading [J]. Acta Materialia, 2019, 167: 149−158.

[15] EGGELER G, HORNBOGEN E, YAWNY A, HECKMANN A, WAGNER M. Structural and functional fatigue of NiTi shape memory alloys [J]. Materials Science and Engineering A, 2004, 378(1/2): 24−33.

[16] PIYAS C, HUSEYIN S. A revisit to atomistic rationale for slip in shape memory alloys [J]. Progress in Materials Science, 2017, 85: 1−42.

[17] HOU Hui-long, EMRAH S, MA Tao, NATHAN J, QIAN Su-xin, CHEIKJ C, DREW S, Al NAILA H, ZHOU Lin, YUNHO H, REINHARD R, VALERY I L, MATTEW J K, MOHSEN A Z, AARON P S, RYAN T O, CUI Jun, ICHIRO T. Fatigue-resistant high-performance elastocaloric materials made by additive manufacturing [J]. Science, 2019, 366(6469): 1116−1121.

[18] XIA Ji, YUKI N, XIAO Xu, TAKUMI O, YUTA K, MAKOKO N, TOSHIHIRO O, RYOSUKE K. Iron-based superelastic alloys with near-constant critical stress temperature dependence [J]. Science, 2020, 369(6505): 855−858.

[19] YEH J W, CHEN S K, LIN S J, GAN J Y, CHIN T S, SHUN T T, TSAU C H, CHANG Shou-yi. Nanostructured high-entropy alloys with multiple principal elements: Novel alloy design concepts and outcomes [J]. Advanced Engineering Materials, 2004, 6(5): 299−303.

[20] ZHANG Bo-wei, ZHANG Ze-qun, DONG Qi-juan, WU Jun-sheng, ZHUANG Ning, ZUO Peng-cheng, LI Xiao-gang. Electrochemical corrosion behavior of nanostructured BCC-$Al_{0.5}CoCrFeNi_{0.4}$ high-entropy alloy in sodium chloride solution [J]. Transactions of Nonferrous Metals Society of China, 2024, 34(6): 1908−1921.

[21] DU Hui, CAI Jia-hong, WANG Ya-song, YAO Jun-qing, CHEN Qiang, CUI Yu, LIU Xin-wang. Effect of partial recrystallization on microstructure and tensile properties of NiFeCoCrMn high-entropy alloy [J]. Transactions of Nonferrous Metals Society of China, 2022, 32(3): 947−956.

[22] RANGANATHAN S. Alloyed pleasures: Multimetallic cocktails [J]. Current Science, 2003, 85(10): 1404−1406.

[23] LI Peng, SUN Hao-tian, LI Chao, WU Bao-sheng, YANG Jiang, JIANG Yu, DONG Hong-gang. A novel strengthening strategy for diffusion bonded joint of $AlCoCrFeNi_{2.1}$ eutectic high entropy alloy to 304 stainless steel [J]. Transactions of Nonferrous Metals Society of China, 2023, 33(7): 2121−2135.

[24] SHI Hong-qi, JI Xiao-di, JIAN Dong-hui, XU Tian-shuo, WANG Chen, TANG Tao, LIU Wen-juan, CAO Zhen-hua. Effect of Mo substitution of Fe on strength and corrosion resistance of $AlCoCrFe_{1-x}NiMo_x$ high-entropy alloys [J]. Transactions of Nonferrous Metals Society of China, 2024, 34(12): 3949−3962.

[25] FIRSTOV G S, KOSORUKOVA T A, KOVAL Y N, ODNOSUM V V. High entropy shape memory alloys [C]//JOSE S J, ANGEL L E. Materials Today: Proceedings. Bilbao, Spain: UPV, 2015: 499−504.

[26] ZHANG Cheng, ZHU Chao-yi, HARRINGTON T, CASALENA L, WANG Hao-ren, SHIN S, VECCHIO K S. Multifunctional non-equiatomic high entropy alloys with superelastic, high damping, and excellent cryogenic properties [J]. Advanced Engineering Materials, 2019, 21(1): 1800941.

[27] LI Shao-hui, CONG Dao-yong, SUN Xiao-ming, ZHANG Yong, CHEN Zhen, NIE Zhi-hua, LI Run-guang, LI Fu-qiang, REN Yang, WANG Yan-dong. Wide-temperature-range perfect superelasticity and giant elastocaloric effect in a high entropy alloy [J]. Materials Research Letters, 2019, 7(12): 482−489.

[28] CANADINC D, TREHERN W, MA Ji, KARAMAN I, SUN Fan-ping, CHAUDHRY Z. Ultra-high temperature multi-component shape memory alloys [J]. Scripta Materialia, 2019, 158: 83−87.

[29] MATSUDA H, SATO H, SHIMOJO M, YAMABE-MITARAI Y. Improvement of high-temperature shape-memory effect by multi-component alloying for TiPd alloys [J]. Materials Transactions, 2019, 60(11): 2282−2291.

[30] MA Ji, KARAMAN I, NOEBE R D. High temperature shape memory alloys [J]. International Materials Reviews, 2010, 55(5): 257−315.

[31] YANG Zhi, CONG Dao-yong, SUN Xian-miao, NIE Zhi-hua, WANG Yan-dong. Enhanced cyclability of elastocaloric effect in boron-microalloyed Ni−Mn−In magnetic shape memory alloys [J]. Acta Materialia, 2017, 127: 33−42.

[32] IBARRA A, CAILLARD D, JUAN J S, NÓ M L. Martensite nucleation on dislocations in Cu−Al−Ni shape memory alloys [J]. Applied Physics Letters, 2007, 90(10): 101907.

[33] CHEN I W, CHIAO Y H. Theory and experiment of martensitic nucleation in ZrO_2 containing ceramics and ferrous alloys [J]. Acta Metallurgica, 1985, 33(10):

1827−1845.

[34] WU Zhi-gang, LIANG Zhi-wen, ZHANG Ya-jiu, LIU Zhu-hong, ZHANG Jun-song, MOTAZEDIAN F, BAKHTIARI S, SHARIAT B S, LIU Yi-nong, REN Yang, YANG Hong. A eutectic dual-phase design towards superior mechanical properties of heusler-type ferromagnetic shape memory alloys [J]. Acta Materialia, 2019, 181: 278−290.

[35] CASALENA L, BUCSEK A N, PAGAN D C, HOMMER G M, BIGELOW G S, OBSTALECKI M, NOEBE R D, MILLS M J, STEBNER A P. Structure-property relationships of a high strength superelastic NiTi−1Hf alloy [J]. Advanced Engineering Materials, 2018, 20(9): 1800046.

[36] AHADI A, SUN Qing-ping. Stress hysteresis and temperature dependence of phase transition stress in nanostructured NiTi: Effects of grain size [J]. Applied Physics Letters, 2013, 103(2): 021902.

[37] WEI Zhi-yang, LIU En-ke, CHEN Jian-hao, LI Yi, LIU Gen-dong, LUO Hong-zhi, XI Xue-kui, ZHANG Hong-wei, WANG Wen-hong, WU Gao-hui. Realization of multifunctional shape-memory ferromagnets in all-d-metal Heusler phases [J]. Applied Physics Letters, 2015, 107(2): 022406.

Ni−Mn−Ti−Fe−Co 共晶高熵合金的超大弹性应变和近恒应力温度依赖性

郭珂良[1]，章 羽[1]，顾江龙[2]，白 静[1,3]，刘 丹[1,3]，Nicola MORLEY[4]，马庆爽[3]，高秋志[3]，左 良[1]

1. 东北大学 材料科学与工程学院 材料各向异性与织构教育部重点实验室，沈阳 110819；
2. 燕山大学 亚稳态材料科学与技术全国重点实验室，秦皇岛 066004；
3. 东北大学秦皇岛分校 资源与材料学院 电介质与电解质功能材料河北省重点实验室，秦皇岛 066004；
4. Department of Material Science and Engineering, University of Sheffield, Sheffield, S1 3JD, UK

摘 要：显著的应力滞后和强烈的温度依赖性限制了超弹性合金的应用。本研究通过将高熵合金原理融入 Ni−Mn−Ti 合金体系，采用电弧熔炼技术开发了一种温度依赖性低的 Ni−Mn−Ti−Fe−Co 超弹性高熵合金。通过全共晶微观结构设计，该合金在 113~433 K 宽温域范围内表现出优异的超弹性稳定性(5%可恢复应变)和极低的滞后能量损耗。此外，该合金在室温条件下经过 12010 次循环加载后仍能保持 5%的完全可逆超弹性变形，同时在 1600 MPa 高应力作用下表现出约 8.2%的显著伪弹性。该合金展现出优异的弹性性能、极低的滞后能量损耗以及宽温域内近恒应力−温度响应等特性源于其独特的共晶微观结构和弱一级相变，从而使其成为跨温度环境超弹性应用的理想候选材料。

关键词：高熵合金；线性超弹性；马氏体相变；共晶组织

(Edited by Wei-ping CHEN)